2015 IEEE/RSJ International Conference on Intelligent Robots and Systems (IROS)
Congress Center Hamburg
Sept 28 - Oct 2, 2015. Hamburg, Germany

Design and fabrication of an insect-scale flying robot for control autonomy

Kevin Y. Ma[1], Pakpong Chirarattananon[2], Robert J. Wood[1]

Abstract— **Without sufficient payload capacity to carry necessary electronic components, flying robots at the scale of insects cannot fly autonomously. Using a simple scaling heuristic to determine a few salient vehicle properties, we develop a vehicle design that possesses the requisite payload capacity for the full suite of required components for control autonomy. We construct the vehicle using state-of-the-art methods, producing a 380 mg vehicle with a 115 mg payload capacity, and demonstrate controlled hovering of the fully-loaded vehicle. The payload-capable vehicle demonstrated here establishes a scalable vehicle design and validates current fabrication methods, laying a foundation for an eventual, fully-integrated robotic system.**

I. Introduction

The number of robotic air vehicles that utilize flapping wing flight has rapidly grown in the last decade. Notable examples include the Aerovironment Nanohummingbird [1] and the DelFly [2]. These two examples in particular have achieved controlled flight, either teleoperated or autonomous. At the scale of small birds, these robotic vehicles have sufficient payload capacity to carry consumer-grade RC components and control electronics.

Robotic flying vehicles at the scale of insects have also been in development for many years, but only in recent years have new innovations in design and manufacturing enabled these tiny robotic systems to be constructed and proven flightworthy. Advances in micromanufacturing emphasizing composite laminate construction of dynamic, small-scale mechanisms [3] have enabled the construction of sophisticated mechanical designs where fabrication precision is crucial to their operation.

Benefiting from these manufacturing innovations, a vehicle design, first introduced in [4] as the "split actuator microrobotic bee", demonstrated the ability to generate both sufficient thrust to lift its own weight and body torques for flight stabilization. With the addition of a closed-loop flight controller, the vehicle successfully demonstrated controlled hovering and basic flight maneuvers [5].

This work was partially supported by the National Science Foundation (award number CCF-0926148) and the Wyss Institute for Biologically Inspired Engineering. Any opinions, findings, and conclusions or recommendations expressed in this material are those of the authors and do not necessarily reflect the views of the National Science Foundation.

[1]Kevin Y. Ma and Robert J. Wood are with the School of Engineering and Applied Sciences and the Wyss Institute for Biologically Inspired Engineering, Harvard University, Cambridge, MA 02138. kevinma@seas.harvard.edu, rjwood@eecs.harvard.edu

[2]P. Chirarattananon is with the Department of Mechanical and Biomedical Engineering, City University of Hong Kong. pakpong.c@cityu.edu.hk

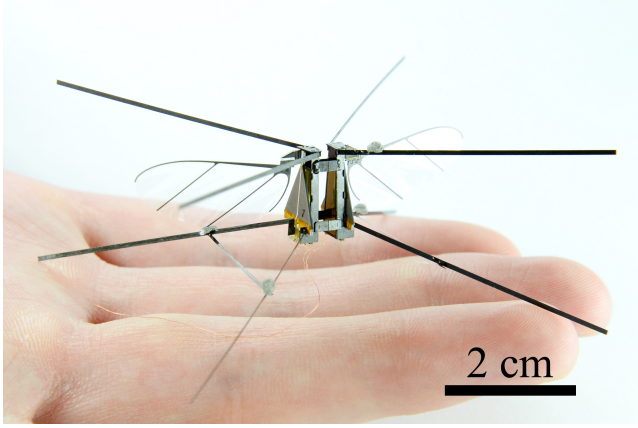

Fig. 1. The prototype robotic flying insect shown here has a wingspan of 5.5 cm and a mass of 380 mg when fully loaded. It has spars extending off the airframe that act as a roll cage to protect the wings from crash damage. Motion tracking markers for control are also attached to these spars.

However, the split actuator microrobotic bee has critical limitations as a research platform for insect-scale robotic flight. A limited payload capacity prevents it from carrying the complete suite of requisite sensors, control and power electronics, and power source necessary for power and control autonomy. Instead, the operation of the vehicle requires a wire tether for power and control signal input. Flight control relies on offboard motion capture for sensory feedback of vehicle dynamics, instead of onboard sensors. And due to a coupling of thrust and torque production, when the vehicle is loaded near its payload capacity limits, control authority is severely reduced.

To create a fully autonomous insect-scale flying robot, a vehicle with more thrust force is required. In this paper, we explore and demonstrate the feasibility of scaling up the established vehicle design to increase its thrust force capability. The system design space for this novel class of flapping-wing micro air vehicle is high-dimensional and complex. To simplify the design problem, we use a scaling heuristic that relies on maintaining properties of the split actuator microrobotic bee. We target the specific payload requirements necessary for control autonomy and develop a mechanical design for the scaled vehicle that is well-suited for electronics integration, utilizing the latest fabrication methods. We construct a 265 mg flying vehicle and demonstrate a 115 mg payload capacity, sufficient for supporting control-autonomous flight with recently-developed, miniaturized electronic components. The new flight result demonstrates feasibility of scaling the established vehicle design and contributes an additional operational reference

TABLE I

ELECTRONIC COMPONENTS NECESSARY FOR CONTROL AUTONOMY

Component	Mass (mg)	Additional physical requirements
"Brain" chip (System-on-Chip microprocessor) [6]	10	
Power electronics [7]	40	Place close to the vehicle base
Inertial measurement unit (IMU) (gyroscope+accelerometer) (Invensense MPU6500)	25	Place close as possible to vehicle center of mass
Optic flow sensor [8]	15	Place downward facing with unobstructed view
Flexible Kapton PCB and electronic integration overhead	10	
Total	100	

TABLE II

DESIGN PARAMETERS FROM THE SPLIT ACTUATOR BEE IN [4]. DESIGN GOALS AND RESULTS FOR THE SCALED UP ROBOTIC BEE.

Vehicle parameter	Units	Split actuator bee	Scale factor	Scaled goals	Scaled results
Flapping frequency	Hz	100	f_{scale} =0.6–0.85	60–85	70
Wing length	mm	15	R_{scale} =1.7	25.5	25.5
Total unloaded robot mass	mg	80	W_{scale} =3	240	265
Total loaded robot mass	mg	115	3	345	380
Measured payload capacity	mg	35	3	105	115
Measured maximum thrust force	mg	140	≈3	414	450
Thrust-to-weight (loaded) ratio	N/A	1.2	hold constant		1.18
Actuator mass fraction	N/A	0.625	hold constant		0.74
Transmission ratio (T)	rad/mm	3.28	hold constant		3.28
Actuator unloaded displacement (δ)	mm	0.85	hold constant		0.85
Actuator base width	mm	1.75			8.606
Wing shape parameter ($\hat{r_2}$)	N/A	<0.55			0.55

point for optimization studies towards a fully autonomous insect-scale flying robot.

II. SYSTEM DESIGN

This paper explores the design and fabrication challenges of scaling an established micro air vehicle design that employs flapping wings, mimicking real flying insects. The scaling laws for flapping-wing micro air vehicles have been explored in theory ([9], [10]) and have provided key relationships between certain vehicle design parameters. However, while they can capture scaling trends, the theoretical models have not been used to generate quantitative specifications for practical vehicle design. Due to lack of fidelity in the modeling, particularly the aerodynamics, accuracy relies on fitting to scale-specific experimental measurements and have questionable accuracy for generating design specifications at other scales [11]. There is little practical guidance for designing and constructing flapping wing air vehicles at the insect scale.

Full system-level optimization of flapping wing air vehicles is a complex, high-dimensional problem with significant interdependence between various design parameters. Considering the aerodynamics of flapping wing flight alone, thrust force production from a single flapping wing predominantly relies on two degrees of freedom—wing flapping and wing pitch rotation [12]. While the aerodynamics are time dependent and unsteady, cycle-averaged, quasi-steady approximations can be used [13]. Force production is dependent on flapping frequency, stroke amplitude, wing pitching amplitude, stroke-to-pitching phasing, and wing geometry—itself parameterized by wing length, wing aspect ratio, and moments of area ([11], [14], [15]). The scaling laws for flapping-wing aerodynamics and system dynamics, in addition to power efficiency considerations [7], need to be reconciled simultaneously in order to identify an optimal design for a high-performance air vehicle.

To accelerate development towards a more payload-capable vehicle, we present a design heuristic that essentially scales the split actuator microrobotic bee vehicle design. By holding constant many properties of an already flightworthy and operational vehicle, we restrict the scaling analysis to a few key parameters, simplifying the design problem.

A. Design goals

The key design specification for this research effort is the payload capacity of the vehicle. We must estimate the target payload requirements of the vehicle. Table I lists the minimum known set of electronic components needed for autonomous flight control, as of the writing of this paper, and the mass of each component. Noticeably missing from Table I is an onboard battery for powering the robotic vehicle. For the sake of near-term research progress, our working goal for this paper is control autonomy—not power autonomy—and assume that electrical power will still be fed to the robot through a wire tether. A more directed effort to reduce battery mass and increase battery energy density is needed prior to adding its mass contribution to the robot's payload.

In addition to the electronics' static payload contribution, we look toward the component mass fractions of the split actuator bee for further design direction. Relevant numbers for this discussion from the previous design are listed in Table II. We hypothesize that a larger scale vehicle would have similar actuator mass fractions, extrapolating from observations on flying insects that found muscle mass fraction to be the best indicator of thrust-to-weight ratio [16]. The split actuator bee has a payload capacity in controlled flight

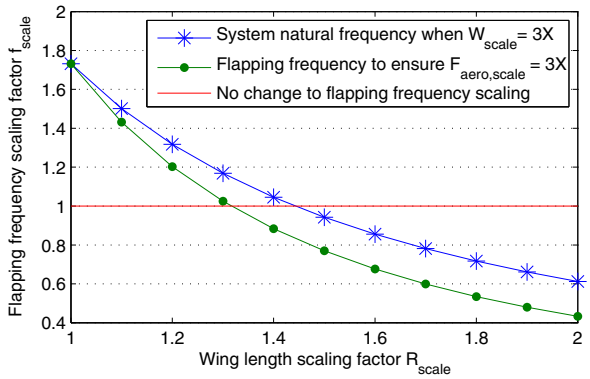

Fig. 2. Scaling trends between flapping frequency and wing length. One is derived from aerodynamic modeling to ensure 3× the thrust force output (Eq.2), and the other is the predicted system natural frequency under 3× the aerodynamic loading (Eq.7).

of about 35 mg [17], on top of a 80 mg unloaded body mass. Based on the 100 mg known total payload needed for control autonomy from Table I, we choose a vehicle with at least 3× the payload capacity of the split actuator bee in order to carry it, or 105 mg. We scale the target body mass similarly by 3× to 240 mg, for a total loaded robot mass of 345 mg. Of the 240 mg body mass, 5/8 would be actuator mass, or 150 mg, and 3/8 would be mechanism and structure mass, or 90 mg.

Additionally, the split actuator bee design has a coupling between thrust force and body torque production. The piezoelectric bimorph cantilever actuators used to power the flapping wings practically operate within voltage bounds from 0–300V, constrained by the ceramic material's strain limits. Within those bounds, a sinusoidal driving signal of varying amplitude and offset can operate. Signal amplitude modulates wing stroke amplitude and thus thrust magnitude. Signal offset modulates the mean wing stroke angle and is used to generate pitch torque in the vehicle by moving the thrust vector fore-aft relative to the vehicle center of mass. If the thrust needed to lift the vehicle is very large, signal amplitudes will increase until maxing out the 300V range. Near this operating point, achievable signal offsets become very limited, which will limit the pitch torque production ability and consequently the flight stability and control authority of the vehicle. Therefore, the maximum thrust output of the vehicle should not be used to calculate the payload capacity; else, the fully loaded vehicle would be unable to produce body pitch torques.

The split actuator bee had a thrust-to-weight ratio of 1.2 when loaded and hovering. Mimicking this, the required maximum thrust force from the scaled vehicle is $1.2 \times 345 = 414$ mg, which is about 3× the maximum measured thrust force from the split actuator bee. The design goals for the scaled vehicle are listed in Table II.

B. Scaling heuristic

The split actuator microrobotic bee design has two flapping wings, each wing independently driven with a separate piezoelectric linear actuator. A four-bar linkage acts as a transmission to amplify the actuator input and produce wing flapping motion. Two separately driven wings enable the vehicle to generate body torques, which is crucial for stabilizing and maneuvering in flight.

To expedite the scaling analysis, we hold constant all key design parameters except the wing length and the flapping frequency. We designate R_{scale} as the wing length scaling factor and f_{scale} as the flapping frequency scaling factor, scaled relative to the split actuator bee parameters. To preserve the wing kinematics of the split actuator bee design, we preserve its transmission ratio of $T = 3.28$ rad/mm and the actuators' unloaded input displacement amplitude to $\delta = 0.85$ mm. For the wing shape, we use the wing morphology from the experiments of [14], with a second wing shape moment $\hat{r_2} = 0.55$ (as defined by [15] as the second moment of area normalized by wing area) and an aspect ratio of 3. This wing shape was found to be an improvement in lift-to-drag ratio over that of the split actuator bee. R_{scale} will scale the wing planform dimensions uniformly.

Aerodynamic forces stemming from flapping wings can be estimated with the blade element method, as described in [10], which assumes aerodynamic force is proportional to local dynamic pressure on the wing. Dividing the flapping wing into chordwise blade elements, the aerodynamic force (either lift or drag) on a single element can be described as:

$$F_{aero} = \frac{1}{2}\rho\left(\dot{\phi}r\right)^2 C_{aero}\left(\alpha\right) S \tag{1}$$

where ρ is the air density; C_{aero} is the aerodynamic force coefficient—a function of instantaneous wing angle of attack α and wing geometry; S is the area of the blade element; and $\left(\dot{\phi}r\right)$ solves for the local velocity of the wing element—it is the product of wing stroke angular velocity $\dot{\phi}$ and local radius r. Total instantaneous force on the wing is found by radial integration over the wing's length R. As we are holding wing kinematics and wing geometry constant, Eq.1 indicates that the aerodynamic force scale factor $F_{aero,scale}$ will scale with R_{scale} and f_{scale} as:

$$F_{aero,scale} \propto R_{scale}^4 \cdot f_{scale}^2 \tag{2}$$

As the actuators are driving the flapping wings, the required blocked force from the actuators F_b to produce a thrust force W was approximated by Eq.14 of [10], reproduced here:

$$F_b = W\frac{\widetilde{C_D}}{\frac{1}{2}\widetilde{C_L}} \cdot T\hat{r_{cp}}R \tag{3}$$

where $\widetilde{C_L}/\widetilde{C_D}$ is the lift-to-drag ratio, T is the transmission ratio, and $\hat{r_{cp}}$ is non-dimensional wing center of pressure radius. As we are fixing the wing kinematics and wing

geometry in this analysis, these parameters are constants. Actuator stiffness k_{act} is the ratio of blocked force F_b to unloaded actuator displacement δ: $k_{act} = {}^{F_b}/_{\delta}$. Actuator displacement is fixed and thus k_{act} is proportional to F_b. Combining with Eq. 3, the scaling relationship between the actuator stiffness scale factor $k_{act,scale}$, thrust force scale factor W_{scale}, and R_{scale} is:

$$k_{act,scale} \propto W_{scale} \cdot R_{scale} \tag{4}$$

Wing inertia is related to the wing morphology. Assuming wing shape does not change, if the wing planform is parameterized by R_{scale} and the wing area dimensions scale uniformly with R_{scale}, then wing inertia I_{wing} should scale with R^4_{scale}. However, for this design exploration, not all wing dimensions are scaled uniformly. A wing consists of a thin structural frame overlaid with a wing membrane, and most of the wing's mass is attributed to the frame. Scaling the frame spar widths uniformly with the wing planform adds wing inertia without contributing significant stiffness. Thus, the wing spar widths are fixed as the wing planform area is scaled. Fixing the wing shape, we use CAD modeling to empirically determine how wing inertia scales with R_{scale}. We determined the scaling law through manual fitting of a power function and found it to be:

$$I_{wing} \propto R^{3.7}_{scale} \tag{5}$$

To determine the wing length and flapping frequency of the scaled vehicle, we apply two constraints in the system modeling. First, the vehicle must generate the target thrust force. Second, the vehicle's flapping-wing system should be operating at its natural frequency. From the analyses performed in [18], we know that this form of flapping-wing mechanism driven with piezoelectric linear actuators can be approximated as a harmonic oscillator. Consequently, there is a distinct natural frequency at which wing stroke amplitudes, and therefore mechanical energy transfer, is greatest. Approximating the system as a harmonic oscillator provides an expression, shown in Eq.6, for the system's natural frequency ω_n. This relationship assumes that the actuators are the primary contributors of system stiffness k_{act} and that the wings are the primary contributors of system inertia I_{wing}.

$$\omega_n = \sqrt{\frac{k_{act}}{I_{wing}}} \tag{6}$$

Consequently, combining Eq.4 and Eq.5 with Eq.6 results in the following scaling relationship between the natural frequency scale factor $\omega_{n,scale}$, W_{scale}, and R_{scale}:

$$\omega_{n,scale} \propto W^{0.5}_{scale} \cdot R^{-1.35}_{scale} \tag{7}$$

To meet both of our design constraints, we equate f_{scale} with $\omega_{n,scale}$ and W_{scale} with $F_{aero,scale}$.

Figure 2 shows curves for Eq.2 and Eq.7 with $F_{aero,scale} = W_{scale} = 3\times$ the magnitude of the split actuator bee, plotted over the f_{scale} vs. R_{scale} space. Any operating point along the aerodynamic scaling curve from Eq.2 should theoretically produce the requisite thrust force, establishing a candidate target wing length and flapping frequency. The curve for the natural frequency scaling suggests that the system natural frequency as estimated in Eq.7 scales slower than the target flapping frequency.

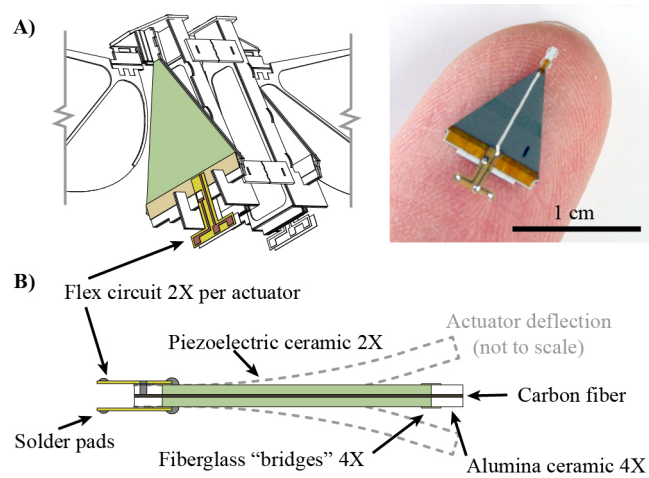

Fig. 3. A) Wiring of the vehicle's piezoelectric bimorph actuators is performed manually. Discrete flex circuit elements are implemented on the actuators to extend the electrical contacts below the vehicle and facilitate manual electrical interfacing. B) The actuators are layered composite beams of piezoelectric ceramic (PZT-5H), alumina ceramic for the base and tip, and carbon fiber for the central elastic layer [19]. Actuator not shown to scale.

We can interpret these curves as an upper and lower bound on our design space. Limited by wing inertia and wing structural limits, we cannot simply increase the flapping frequency of the split actuator bee to attain greater thrust force. An alternative is to increase wing length (and thus wing inertia) and flap at a lower frequency. As illustrated in Figure 2, aerodynamic scaling dictates a wing length 1.3× longer to ensure a flapping frequency scaling of less than 1. Natural frequency scaling suggests a wing length 1.5× longer to ensure the same.

Weighing in our intuition on structural limits of our current wing fabrication methods, we choose a wing length scaling of 1.7× as a starting point for exploration into scaled vehicle fabrication. With 1.7× longer wings, a 0.6× lower flapping frequency is sufficient to generate the target thrust force; a 0.85× lower natural frequency is also predicted. We anticipate the actual operating frequency of the vehicle will fall in between these predictions. Table II lists the target design parameters for the scaled up vehicle.

III. Vehicle Fabrication

We utilize our latest fabrication methods to construct the prescribed vehicle design. In determining our methods, we are reconciling the need for high-performance components with the efficiency of their production. To effectively support further system experimentation, we are interested in producing on the order of 10 vehicles. Ideally, the vehicles should be identical in properties and performance. Prior experience

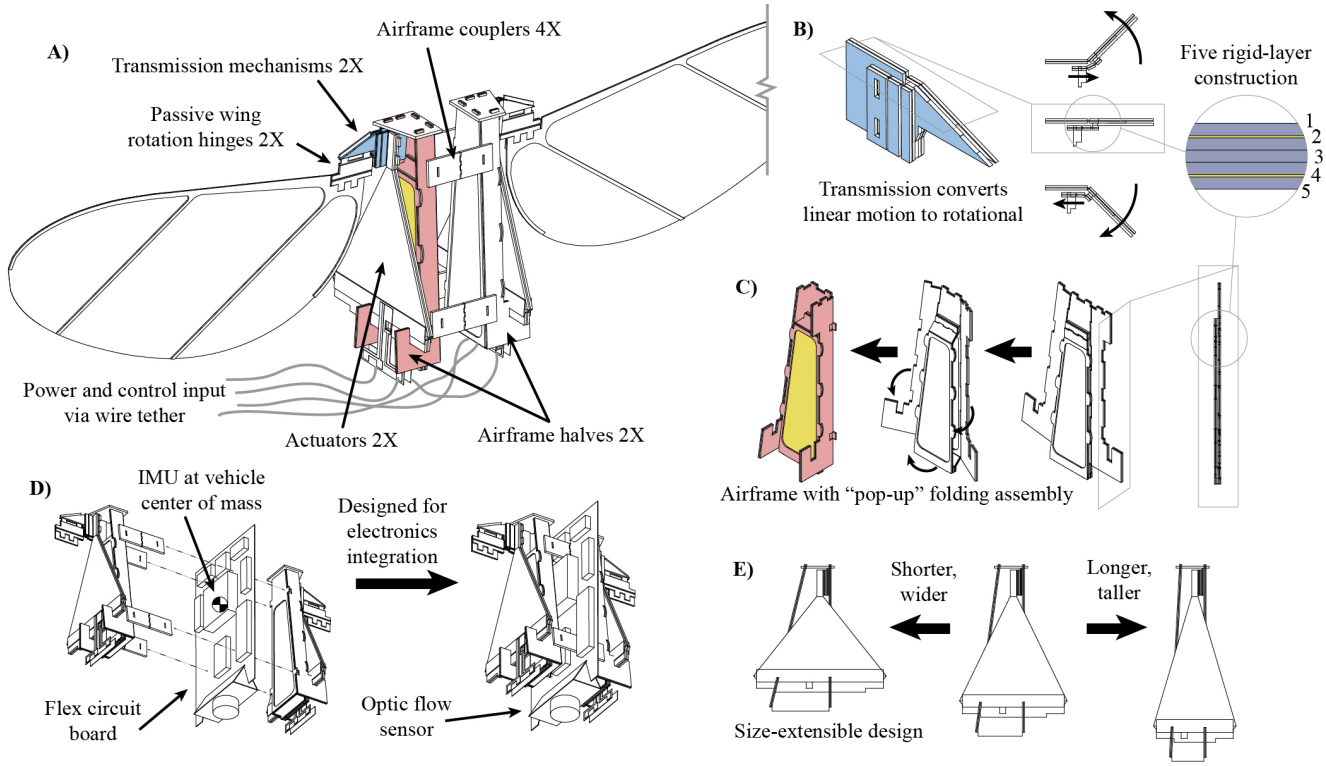

Fig. 4. Construction details for the robotic flying insect. A) Assembly of components that make up the vehicle. B) The transmission converts the nominally linear actuator tip motion to a rotational flapping motion. It is constructed with laminated layers of rigid carbon fiber composite and flexible polyimide film and consists of five rigid layers. C) The airframe is a rectangular thin-walled tube structure, designed for efficient bending and torsional resistance. Similarly with the transmission, it consists of five rigid layers of carbon fiber composite and can be fabricated simultaneously with the transmission. The design is a pop-up structure for ease of assembly. Polyimide film membrane (colored yellow) stretches across the broad faces—a semi-monocoque airframe. D) Extensibility for electronic integration. The electronic components will populate a flex circuit board that resides in the central plane of the vehicle, establishing a straightforward method for packaging the components and achieving a balanced mass distribution in the vehicle. The IMU can be designed to coincide with the vehicle's center of mass. E) Extensibility for scaling optimizations. The airframe dimensions can be easily modified to accomodate any actuator size around this scale regime.

suggests this is very difficult to achieve, but as methods continue to be refined, we gradually approach this ideal. The mechanical system can be divided into separate components, each with distinct manufacturing considerations.

A. Wings

The wings are fabricated in batches as thin polyester film laminated over a monolithic, laser-machined carbon fiber frame, a method identical to what was used for the split actuator bee. They should be lightweight, stiff, resilient to aerodynamic loading, and efficient to reproduce. The wing shape is fixed as described in Section 2B.

Because the new vehicle will generate more thrust force, the wings will experience greater aerodynamic loading. As a simple approximation, if we are using the 1.7× longer wings to generate 3× more aerodynamic force, this translates to 5.1× greater bending moment at the wing base due to aerodynamic loading. In this initial effort, we increased the wing frame's carbon fiber beam thickness by 50%, increasing the bending stiffness by 3.4×. Experiments indicate that the wings are stiff enough to withstand the aerodynamic loading without bending. However, without further characterization studies, we are not certain to what extent the new wings are sufficiently robust. To prevent wing damage during operation, we add a roll cage consisting of thin carbon fiber spars that prevent the wings from hitting the ground, as seen in Figure 1.

B. Actuators

The piezoelectric ceramic bimorph actuators used in the vehicle are fabricated according to the design and fabrication methods described in [19] and [20]. We use the actuator model from [20] to determine the geometry of the new actuators. Because the transmission and actuator displacement properties are fixed, the increased wing loading (Section 3A) directly translates to a 5.1× larger blocked force requirement for the actuators. Actuator blocked force is proportional to the nominal actuator width [20]. To meet the greater force requirements, the new actuators are larger: the piezoelectric ceramic layer is 8.332 mm in length and 8.606 mm in base width. Figure 3 illustrates the actuators' design and implementation in the vehicle.

C. Transmission

The transmission is a four-bar linkage that converts the motion of the actuator tip to flapping wing motion. In the

split actuator bee, the transmission's construction required a delicate manual folding and assembly procedure that was vulnerable to human error. In the new vehicle, we rely on the layered, pop-up manufacturing method from [3] to produce the four-bar mechanism; this outputs a fully assembled transmission as a 5 rigid-layer, laminated structure with no manual assembly steps. Figure 4B illustrates the operation and construction of the transmission linkage. As described in Section 2B, the transmission ratio remains the same as that of the split actuator bee.

Similar to the split actuator bee, the wings are attached to the transmissions through an elastically-deforming, passive rotation hinge in series, which provides the unactuated wing pitch degree-of-freedom. Wing pitching motion is passively modulated by the interaction of aerodynamic forces with the wing's inertia and elastic hinge stiffness. The passive rotation hinge is shown in Figure 4A. They are fabricated separately from the transmissions and wings to allow for interchangeability of parts and to support experimentation of wing mechanics.

D. Airframe

The airframe is the vehicle's mechanical ground structure. It must rigidly ground the actuators and transmissions and resist bending and twist-loading with minimal deformation, while also remaining lightweight. To address these design constraints, we use a hollow beam construction to increase structural efficiency. The materials used are carbon fiber and Kapton polyimide film. This composite structure is constructed using the pop-up manufacturing method [3] and can also be produced as a 5 rigid-layer laminate, simultaneously with the transmissions.

As this vehicle is explicitly designed for electronics integration, the airframe is designed as two halves with the hull space in between to house the electronics payload. Each half consists of an airframe, actuator, transmission, and wing, and the two halves are mirror images of each other. These two halves are rigidly coupled together with additional coupler beams.

The design must be extensible for electronics integration, based on known placement needs for certain electronic components. Some electronic components require specific orientations and placement on the vehicle structure, as described in Table I. In particular, the IMU benefits from being placed at the vehicle's center of mass to reduce translational vibration [17]. To account for a range of possible component placements, simplify the component packaging problem, and reduce structural mass, we envision placing all electronic components on a single, planar flex circuit. This flex circuit resides in the midplane of the vehicle. Knowing the vehicle structure's center of mass and the mass distribution of the populated flex circuit, we can design the flex circuit such that the IMU coincides with the center mass of the fully assembled vehicle. Figure 4D illustrates this concept.

The airframe secures the actuator base at two points. This simple mounting scheme and the design of the airframe can be easily adjusted to support a range of actuator sizes (see Figure 4E).

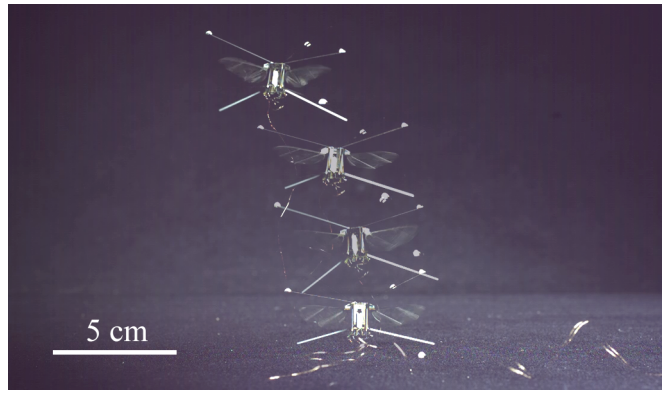

Fig. 5. Stationary hovering flight of the 265 mg robot with a 115 mg payload—380 mg total. The robot hovered 10 cm above the ground for 4 seconds. Strobed positions of the flight ascent are shown.

IV. Results

We were able to perform a controlled hovering flight with a 115 mg dummy payload onboard. We use the experimental setup presented in [5], which relies on an array of external motion tracking cameras (Vicon, Oxford, UK) to observe the vehicle's position and attitude in flight. This real time tracking is used with a closed-loop flight controller implemented on an offboard desktop computer and adjusted for the new vehicle's properties, to calculate appropriate control inputs for specified flight behavior. The method of driving the wings for flight stability is described in [4] and [5]. Power and control signals are fed to the vehicle through a wire tether. This wire tether was shown to have a negligible effect on the flight dynamics of the vehicle [21].

The robotic vehicle was able to lift off and maintain a stationary hover about a setpoint with minimal deviations in position and attitude, thus achieving the design goal of 105 mg payload capacity. The natural frequency of the flapping mechanism was experimentally determined to be 70 Hz—within the predicted range from Section 2B. Using a custom-built capacitive force sensor, we measured a maximum thrust force of 450 mg. The properties of the completed vehicle are summarized in Table II. An image of the hovering flight is shown in Figure 5. The full flight result is shown in the supplemental video.

V. Discussion

The controlled flight demonstration confirms that this particular vehicle design can be control autonomous, based on the mass estimates of the required electronic components. Our measured maximum thrust force exceeds what is required to lift and control the robotic vehicle. We consider these results to be preliminary. More characterization of the vehicle design is required, including stress testing for the true maximum thrust force.

Our current vehicle fabrication methods are adequately repeatable though assembly errors and variability are still

introduced. This is inconvenient, as the flight controller gains need to be specifically tuned for individual vehicles. Alignment fixtures and additional pop-up, auto-aligning design features may enable more repeatable assembly. Mechanisms for mechanical trimming could be implemented in the vehicle design itself. Further improvements to the mechanical design include refined wing design and more systematic airframe structural design.

In Table II, we see that the total unloaded robot mass and actuator mass fraction was greater than the scaling target. This may indicate that our actuators are oversized for the target payload capacity and could account for the greater-than-predicted thrust forces. The larger thrust force could also be attributed to the change in wing shape from the split actuator bee.

Modeling uncertainty likely exists in the system dynamics relation in Eq.6. The wing inertia relation in Eq.5 does not account for added mass contribution from the acceleration of surrounding air. This is a significant inertial component [13] but not straightforward to introduce into the scaling heuristic. Our heuristic also ignores aerodynamic damping because of the difficulty in assigning a fixed damping coefficient for constantly accelerating flapping-wings. The system dynamics study in [18] highlighted the use of the damped resonant frequency for better predicting system behavior.

Nevertheless, experiments have verified that the aerodynamic modeling based on the quasi-steady blade element method can robustly capture scaling trends [11], [14]. This analysis is further simplified by maintaining previously-verified wing kinematics. Thus, the scaling heuristic relies on the aerodynamic modeling for vehicle scaling while the natural frequency analysis provides an indication of how the system behavior would change at larger scales. A full system optimization of the vehicle system would include more detailed modeling and scaling trends derived from first-principles in order to prescribe an optimized vehicle design.

At conception, this vehicle was intended for electronics integration, and this has significantly influenced the structural design. The payload capacity as-is provides utility for the realization of control autonomy in insect-scale flying robots. We have demonstrated how the established split actuator bee vehicle design can be successfully scaled and fabricated using our current methods. A more-developed modeling and optimization effort can further refine the design and will leave the integration of an onboard power source as the last major research hurdle toward control and power autonomous operation of robotic flying insects. Candidate technologies for the power source include micro fuel cells, solar cells, conventional-, and novel-structured lithium ion batteries [22].

Acknowledgments

The authors thank Farrell Helbling for assisting with the controlled flight experiments and for fruitful discussions.

References

[1] M. Keennon, K. Klingebiel, H. Won, and A. Andriukov, "Development of the nano hummingbird: A tailless flapping wing micro air vehicle," in *AIAA Aerospace Sciences Meeting*, 2012, pp. 1–24.

[2] D. Lentink, S. R. Jongerius, and N. L. Bradshaw, "The scalable design of flapping micro-air vehicles inspired by insect flight," in *Flying insects and robots*. Springer, 2010, pp. 185–205.

[3] P. S. Sreetharan, J. P. Whitney, M. D. Strauss, and R. J. Wood, "Monolithic fabrication of millimeter-scale machines," *Journal of Micromechanics and Microengineering*, vol. 22, no. 5, p. 055027, 2012.

[4] K. Y. Ma, S. M. Felton, and R. J. Wood, "Design, fabrication, and modeling of the split actuator microrobotic bee," in *Intelligent Robots and Systems (IROS), 2012 IEEE/RSJ International Conference on*. IEEE, 2012, pp. 1133–1140.

[5] K. Y. Ma, P. Chirarattananon, S. B. Fuller, and R. J. Wood, "Controlled flight of a biologically inspired, insect-scale robot," *Science*, vol. 340, no. 6132, pp. 603–607, 2013.

[6] X. Zhang, T. Tong, D. Brooks, and G.-Y. Wei, "Evaluating adaptive clocking for supply-noise resilience in battery-powered aerial microrobotic system-on-chip," 2014.

[7] M. Karpelson, G.-Y. Wei, and R. J. Wood, "Milligram-scale high-voltage power electronics for piezoelectric microrobots," in *Robotics and Automation, 2009. ICRA'09. IEEE International Conference on*. IEEE, 2009, pp. 2217–2224.

[8] P.-E. Duhamel, N. O. Perez-Arancibia, G. L. Barrows, and R. J. Wood, "Biologically inspired optical-flow sensing for altitude control of flapping-wing microrobots," *Mechatronics, IEEE/ASME Transactions on*, vol. 18, no. 2, pp. 556–568, 2013.

[9] C. P. Ellington, "The novel aerodynamics of insect flight: applications to micro-air vehicles," *Journal of Experimental Biology*, vol. 202, no. 23, pp. 3439–3448, 1999.

[10] J. Whitney and R. Wood, "Conceptual design of flapping-wing micro air vehicles," *Bioinspiration & biomimetics*, vol. 7, no. 3, p. 036001, 2012.

[11] ——, "Aeromechanics of passive rotation in flapping flight," *Journal of Fluid Mechanics*, vol. 660, pp. 197–220, 2010.

[12] S. N. Fry, R. Sayaman, and M. H. Dickinson, "The aerodynamics of free-flight maneuvers in drosophila," *Science*, vol. 300, no. 5618, pp. 495–498, 2003.

[13] C. Ellington, "The aerodynamics of hovering insect flight. i. the quasi-steady analysis," *Philosophical Transactions of the Royal Society B: Biological Sciences*, vol. 305, no. 1122, pp. 1–15, 1984.

[14] A. L. Desbiens, Y. Chen, and R. J. Wood, "A wing characterization method for flapping-wing robotic insects," in *Intelligent Robots and Systems (IROS), 2013 IEEE/RSJ International Conference on*. IEEE, 2013, pp. 1367–1373.

[15] C. Ellington, "The aerodynamics of insect flight. ii. morphological parameters," *Phil. Trans. R. Soc. Lond. B*, vol. 305, pp. 17–40, 1984.

[16] J. H. Marden, "Maximum lift production during takeoff in flying animals," *Journal of Experimental Biology*, vol. 130, no. 1, pp. 235–258, 1987.

[17] S. B. Fuller, E. F. Helbling, P. Chirarattananon, and R. J. Wood, "Using a MEMS gyroscope to stabilize the attitude of a fly-sized hovering robot," in *IMAV 2014: International Micro Air Vehicle Conference and Competition 2014, Delft, The Netherlands, August 12-15, 2014*. Delft University of Technology, 2014.

[18] B. M. Finio, N. O. Pérez-Arancibia, and R. J. Wood, "System identification and linear time-invariant modeling of an insect-sized flapping-wing micro air vehicle," in *Intelligent Robots and Systems (IROS), 2011 IEEE/RSJ International Conference on*. IEEE, 2011, pp. 1107–1114.

[19] N. T. Jafferis, M. J. Smith, and R. J. Wood, "Design and manufacturing rules for maximizing the performance of polycrystalline piezoelectric bending actuators," *Smart Materials and Structures*, 2015.

[20] R. Wood, E. Steltz, and R. Fearing, "Optimal energy density piezoelectric bending actuators," *Sensors and Actuators A: Physical*, vol. 119, no. 2, pp. 476–488, 2005.

[21] S. B. Fuller, M. Karpelson, A. Censi, K. Y. Ma, and R. J. Wood, "Controlling free flight of a robotic fly using an onboard vision sensor inspired by insect ocelli," *Journal of The Royal Society Interface*, vol. 11, no. 97, p. 20140281, 2014.

[22] K. Sun, T.-S. Wei, B. Y. Ahn, J. Y. Seo, S. J. Dillon, and J. A. Lewis, "3D printing of interdigitated Li-Ion microbattery architectures," *Advanced Materials*, vol. 25, no. 33, pp. 4539–4543, 2013.